Effect of roof impacts on coupling between wave response and shloshing in tanks of LNG-carriers

Bernard Molin, Fabien Remy, A. Ledoux, N. Ruiz

EFFECT OF ROOF IMPACTS ON COUPLING BETWEEN WAVE RESPONSE AND SLOSHING IN TANKS OF LNG-CARRIERS

Bernard Molin*
Fabien Remy
Ecole Centrale Marseille & IRPHE
13 451 Marseille cedex 20
France
Email: bernard.molin@ec-marseille.fr
fabien.remy@ec-marseille.fr

Alain Ledoux
Nicolas Ruiz
Principia R.D.
13 705 la Ciotat cedex
France
Email: alain.ledoux@principia.fr
nicolas.ruiz@principia.fr

ABSTRACT

An experimental campaign is reported on the wave response of a rectangular barge supporting two rectangular tanks partly filled with water. Flat and chamfered tank roofs are successively tested, at varying heights above the free surfaces inside the tanks. The tests are carried out in irregular wave systems coming from abeam. The measured barge roll and sloshing motions in the tanks are compared with numerical results from a linearized potential flow model. Good agreement is reported in mild seastates. Nonlinear effects, associated with large amplitude sloshing motion and/or roof impacts, are investigated.

INTRODUCTION

In [1] a theoretical model was proposed to couple liquid motion in tanks and sea-keeping of the floating support. This model relies on linearized potential flow theory and decomposes the sloshing motion in tanks over a finite number of modes, with the modal amplitudes obeying simple spring-mass equations. Numerical implementation was first performed in 2D configurations, then a specific module was developed within the DIODORE^{TM} software of Principia. Dedicated experiments were performed in the wavetank BGO-First with a rectangular barge equipped with two rectangular tanks, submitted to irregular beam seas (see figure 1). Different water levels in the tanks were achieved, and difference surface conditions (smooth or rough). Good agreement was obtained between experimental and numerical response amplitude operators (RAOs), both for the roll motion of the barge and for the liquid motion in the tanks, except at very low filling heights.

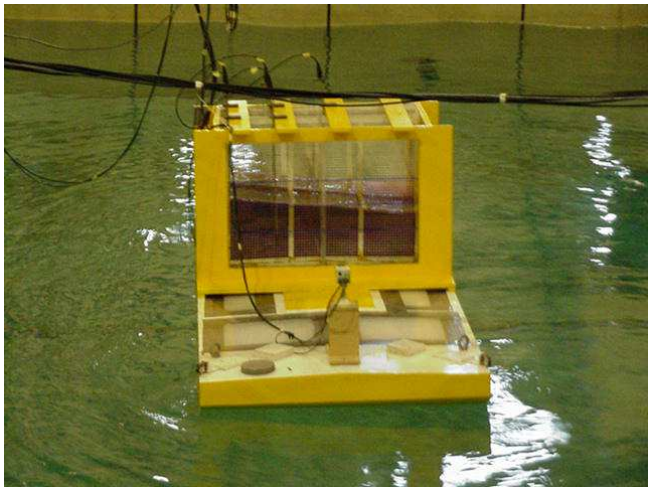

Figure 1. BARGE MODEL IN THE BASIN (FROM [1]).

In these experiments, as can be seen in figure 1, the tanks had no roofs.

*Address all correspondence to this author.

Recently a new series of experiments was carried out, with the same model, and with the tanks fitted with roofs. The water level was kept the same throughout the tests, while the roofs were set at different heights above the free surfaces. The roofs were successively flat and chamfered.

In this paper we first recall the theoretical model presented in [1]. Then we describe the new experiments performed and we present a detailed comparison between the measurements and the computational results, obtained with a 2D semi-analytical model and with the DIODORE^{TM} software.

THEORY

Natural sloshing modes

The first step is to determine the natural sloshing modes for each tank, at its filling height. This means obtaining the non-trivial solutions of the following boundary value problem:

$$\Delta\varphi = 0 \quad \text{within the fluid volume} \tag{1}$$
$$\nabla\varphi \cdot \vec{n} = 0 \quad \text{on the walls } S_C \tag{2}$$
$$g\,\varphi_z - \omega^2\,\varphi = 0 \quad \text{at the free surface } S_F \tag{3}$$

where

$$\Phi(x,y,z,t) = \varphi(x,y,z)\ \sin(\omega t + \theta)$$

For a two-dimensional rectangular tank, of length b and height of liquid h, the eigen-modes are given by

$$\Phi_n = -\frac{A_{n0}\,g}{\omega_n}\ \frac{\cosh\lambda_n(z+h)}{\cosh\lambda_n h}\ \cos\lambda_n y\ \sin(\omega_n t + \theta_n) \tag{4}$$

where the natural frequencies ω_n are

$$\omega_n^2 = g\,\lambda_n\ \tanh\lambda_n\,h \qquad \text{with} \qquad \lambda_n = \frac{n\,\pi}{b} \tag{5}$$

and the free surface elevation is

$$\eta_n(y,t) = A_{n0}\ \cos\lambda_n y\ \cos(\omega_n t + \theta_n) \tag{6}$$

(in a reference system Oxz such that O is located at the intersection of the free surface and one of the vertical walls).

For a tank of general shape the eigen-modes can be obtained with a numerical software.

It is easy to show that the potentials $\varphi_n(x,y,0)$ form an orthogonal and complete basis at the free surface.

As a result the free surface elevation can be expanded as

$$\eta(x,y,t) = \sum_n A_n(t)\ \zeta_n(x,y) \tag{7}$$

where

$$\zeta_n(x,y) = \frac{\omega_n}{g}\ \varphi_n(x,y,0) \tag{8}$$

(the elementary potentials φ_n being normalized so that, for instance, $\max\ \zeta_n(x,y) = 1$).

The velocity potential within the tank is then given by

$$\Phi(x,y,z,t) = -\sum_n \left(\int_0^t A_n(\tau)\,d\tau \right) \omega_n\,\varphi_n(x,y,z) \tag{9}$$

This is correct under the condition that the tank be motionless, since Φ satisfies the homogeneous Neumann condition at the walls.

Elementary forced motion problems

Now we consider the tank undergoing forced motion along one of its 6 degrees of freedom. The elementary problems to be solved are

$$\Delta\varphi_j = 0 \qquad \text{fluid domain} \tag{10}$$
$$\nabla\varphi_j \cdot \vec{n} = N_j \qquad \text{at } S_C \tag{11}$$
$$g\,\varphi_{jz} - \omega^2\,\varphi_j = 0 \qquad \text{at } S_F\ (z=0) \tag{12}$$

the frequency ω being given. N_j stands for one component of the generalized normal vector.

The potential φ_j is looked for as:

$$\varphi_j = \widetilde{\phi}_j + \psi_j \tag{13}$$

where $\widetilde{\phi}_j$ is the infinite frequency "radiation" potential, which satisfies

$$\Delta\widetilde{\phi}_j = 0 \qquad \text{fluid domain} \tag{14}$$
$$\nabla\widetilde{\phi}_j \cdot \vec{n} = N_j \qquad \text{at } S_C \tag{15}$$
$$\widetilde{\phi}_j = 0 \qquad \text{at } S_F\ (z=0) \tag{16}$$

It ensues that the additional potential ψ_j satisfies

$$\Delta\psi_j = 0 \qquad \text{fluid domain} \tag{17}$$

$$\nabla\psi_j \cdot \vec{n} = 0 \qquad \text{at } S_C \tag{18}$$

$$g\,\psi_{jz} - \omega^2\,\psi_j = -g\,\widetilde{\phi}_{jz} \qquad \text{at } S_F\ (z=0) \tag{19}$$

The solution is straight-forward when one has projected $\widetilde{\phi}_{jz}(x,y,0)$ on the basis $\varphi_n(x,y,0)$:

$$\begin{aligned}\widetilde{\phi}_{jz}(x,y,0) &= \sum_n \frac{\iint_{S_F} \widetilde{\phi}_{jz}\,\varphi_n\,\mathrm{d}S}{\iint_{S_F}\varphi_n^2\,\mathrm{d}S}\,\varphi_n(x,y,0)\\ &= \sum_n \gamma_{jn}\,\varphi_n(x,y,0).\end{aligned} \tag{20}$$

One obtains

$$\psi_j(x,y,z) = -g\,\sum_n \frac{\gamma_{jn}}{\omega_n^2-\omega^2}\,\varphi_n(x,y,z) \tag{21}$$

The sum $\widetilde{\phi}_j + \psi_j$ is the velocity potential resulting from a unit velocity amplitude along degree of freedom j. When one relates the amplitude A_n of the sloshing motion n to the motion amplitude X_j, one obtains the RAO

$$A_n/X_j = -\frac{\omega^2\,g\,\gamma_{jn}}{\omega_n\,(\omega_n^2-\omega^2)} = -\frac{\omega^2}{\omega_n^2-\omega^2}\,D_{nj} \tag{22}$$

It is equivalent to write that $A_n(t)$ obeys the pendulum equation

$$\ddot{A}_n + \omega_n^2\,A_n = D_{nj}\,\ddot{X}_j \tag{23}$$

which remains valid when $X_j(t)$ is not harmonic since the D_{nj} coefficients do not involve the frequency ω. They are defined by

$$D_{nj} = \frac{g}{\omega_n}\,\frac{\iint_{S_F}\widetilde{\phi}_{jz}\,\varphi_n\,\mathrm{d}S}{\iint_{S_F}\varphi_n^2\,\mathrm{d}S} \tag{24}$$

Making use of the integral identities

$$\iint_{S_F}\widetilde{\phi}_{jz}\,\varphi_n\,\mathrm{d}S = \iint_{S_F}\left(\widetilde{\phi}_{jz}\,\varphi_n - \widetilde{\phi}_j\,\varphi_{nz}\right)\mathrm{d}S$$

$$= -\iint_{S_C}\left(\nabla\widetilde{\phi}_j\cdot\vec{n}\,\varphi_n - \nabla\varphi_n\cdot\vec{n}\,\widetilde{\phi}_j\right)\mathrm{d}S$$

$$= -\iint_{S_C} N_j\,\varphi_n\,\mathrm{d}S \tag{25}$$

we obtain the alternative expression

$$D_{nj} = -\frac{g}{\omega_n}\,\frac{\iint_{S_C}\varphi_n\,N_j\,\mathrm{d}S}{\iint_{S_F}\varphi_n^2\,\mathrm{d}S} \tag{26}$$

Hydrodynamic forces at the walls

From the above analysis the velocity potential within the tank is given by

$$\begin{aligned}\Phi(x,y,z,t) = &-\sum_n\left(\int_0^t A_n(\tau)\,\mathrm{d}\tau\right)\,\omega_n\,\varphi_n(x,y,z)\\ &+\sum_{j=1}^{6}\dot{X}_j(t)\,\widetilde{\phi}_j\end{aligned} \tag{27}$$

The hydrodynamic pressure being

$$p = -\rho\,\Phi_t = \rho\sum_n A_n(t)\,\omega_n\,\varphi_n - \rho\sum_{j=1}^{6}\ddot{X}_j(t)\,\widetilde{\phi}_j \tag{28}$$

the hydrodynamic loads are given by

$$\vec{F} = \iint_{S_C} p\,\vec{n}\,\mathrm{d}S \tag{29}$$

$$\vec{C} = \iint_{S_C} p\,\vec{r}\wedge\vec{n}\,\mathrm{d}S \tag{30}$$

i.e., introducing the generalized force tensor $\vec{F} = (\vec{F},\vec{C})$:

$$\vec{F} = \sum_n A_n(t)\,\vec{f}_n - \mathbf{M_a}(\infty)\,\ddot{\vec{X}} \tag{31}$$

where $\mathbf{M_a}(\infty)$ is the infinite frequency added mass matrix and

$$f_{nj} = \rho\,\omega_n\iint_{S_C}\varphi_n\,N_j\,\mathrm{d}S \tag{32}$$

It may be noticed that the f_{nj} and D_{nj} coefficients are obtained through the same integral over S_C and that they are simply related:

$$D_{nj} = -\frac{g}{\rho}\,\frac{f_{nj}}{\omega^2{}_n\iint_{S_F}\varphi^2{}_n\,\mathrm{d}S} \tag{33}$$

Furthermore, the following identity, helpful for numerical checks, holds

$$\mathbf{M_a}_{ij}(\infty) - \mathbf{M_a}_{ij}(0) = \sum_n \frac{f_{ni}\, D_{nj}}{\omega_n^2}$$

$$= -\rho\, g \sum_n \frac{\left[\iint_{S_C} \varphi_n\, N_i \,\mathrm{d}S\right]\ \left[\iint_{S_C} \varphi_n\, N_j \,\mathrm{d}S\right]}{\omega_n^2\ \iint_{S_F} \varphi_n^2 \,\mathrm{d}S} \qquad (34)$$

Coupled motion equations

All there remains to do is to couple the motion equations of the barge and the pendulum equations for the sloshing motions in each tank. In the latter linear and quadratic dissipation terms are introduced, giving

$$\ddot{A}_{in} + B_{1in}\,\dot{A}_{in} + B_{2in}\,\dot{A}_{in}\,|\dot{A}_{in}| + \omega_{in}^2\,A_{in} = \sum_{j=1}^{6} D_{inj}\,\ddot{X}_{ij} \qquad (35)$$

Here the suffix i stands for tank number i and X_{ij} is the j-component of the barge motion, at tank i.

The damping terms can be related to frictional energy losses at the walls (see [1]), or, heuristically, to other sources of internal energy dissipation like wave breaking. Energy dissipation in the coupled mechanical system is also ensured by outer radiation damping and by the viscous damping in roll, which is found to play the dominant role. In the numerical model, the viscous damping moment in roll is expressed by

$$C_{v4} = -\frac{1}{2}\,\rho\, C_d\, B^4\, L\, |\dot{\alpha}|\, \dot{\alpha} \qquad (36)$$

where C_d is a non-dimensional coefficient, B is the beam of the barge, L its length and $\dot{\alpha}$ the roll velocity.

In the resolution, the so-called "stochastic linearization" is applied, meaning that the damping moment is written as

$$C_{v4} = -\sqrt{\frac{2}{\pi}}\,\rho\, C_d\, B^4\, L\, \sigma_{\dot{\alpha}}\, \dot{\alpha} \qquad (37)$$

where $\sigma_{\dot{\alpha}}$ is the standard deviation of the roll velocity. This procedure ensures identical energy dissipations for gaussian processes.

It ensues that the combined equations of motion need to be solved through iterations, for a given sea-state specified by its energy spectrum. At each iteration the standard deviation $\sigma_{\dot{\alpha}}$ of the roll velocity is re-actualized. Convergence is usually reached within a few iterations. The same procedure is applied to the quadratic damping terms in equations (35).

EXPERIMENTAL CAMPAIGN

The experiments were carried out in the wave tank BGO-First, at la Seyne sur mer. This facility is 16 m wide, for a total length around 40 m. Thanks to a false bottom the water-depth can be varied from near 0 up to 5 m. During the experiments, it was set at 3 m.

The same barge model as in the previous campaign was used. It is 3 m long and 1 m wide, with a depth of 26.7 cm. The draft during the tests was 11 cm.

Two identical rectangular glass tanks were used, 80 cm long and 25 cm wide, with a height of 60 cm. These values refer to the internal dimensions. The two tanks were installed on the deck, with their lengths in the transverse direction of the barge model. They were filled with water at a depth of 29 cm, meaning 116 kg of water, while the mass of the model with the empty tanks (including instrumentation) was 176 kg. This is a configuration that was considered in the previous campaign; the only difference is that, due to the weight of tank roofs, force sensors and aerial camera, in this new campaign the total weight is a little bit larger (by 5 kg) and the center of gravity somewhat higher (29 cm above keel line vs. 24 cm). The roll radius of inertia of the barge with the tanks empty was around 42 cm.

The roofs in the tanks could be adjusted in position. They were located successively at 29 cm (no free surface), 35 cm, 40 cm and 45 cm above the tank floors, meaning airgaps of 0 cm, 6 cm, 11 cm and 16 cm. Then the roofs were fitted with chamfered corners, 18 cm $\times$ 18 cm. Successive roof positions at 35 cm, 40 cm, 45 cm and 50 cm above tank floors were then achieved, meaning airgaps of 6 cm, 11 cm, 16 cm and 21 cm. At 16 cm, the bottom ends of the chamfers were slightly below the still water level (by 2 cm), the length of which was shortened by 4 cm. At 11 cm the still water length was reduced by 14 cm, down to 66 cm. At 6 cm it was reduced by 24 cm, down to 56 cm. These are the three cases when the natural sloshing modes in the tank must be determined numerically.

The barge was moored by an horizontal cables + springs system. The resulting natural period in sway was 10.8 s.

Instrumentation consisted in the optical tracking RODYM system, giving the 6 dof motion with a very high accuracy. The free surface in one of the tanks was tracked optically with an onboard video camera. Image processing yielded the experimental modal amplitudes. Another onboard camera was set above one of the tanks, shooting down vertically so as to visualize the wetted area on the underside of the transparent roof. The vertical loads on the other roof were measured through a combination of 3 force sensors.

The tests were run in irregular waves coming from abeam. The seastates were calibrated without the barge model. The spectra were of JONSWAP type, with $\gamma = 2$, and peak periods T_P of 1.6 s and 2 s. At 1.6 s, the specified H_S values were 6 cm, 9 cm and 12 cm (seastates Irr1, Irr2, Irr3). At 2 s they were 8 cm,

12 cm and 16 cm (Irr4, Irr5, Irr6). These are somewhat stronger seastates than in the previous campaign (see [1]); at a scale of 1:50, the full-scale significant waveheights would be 3 m, 4.5 m, 6 m at a peak period of 11.3 s, and 4 m, 6 m, 8 m at a peak period of 14.1 s. The test duration was 600 s and the sampling rate was 100 Hz.

In this paper we focus on the first three seastates, for which the peak frequency is closer to the natural frequencies of the coupled roll and sloshing motions.

COMPARISONS BETWEEN EXPERIMENTAL AND NUMERICAL RESULTS

Closed tanks

We start with the case when the roofs are lowered down to the free surfaces, inhibiting their motions. Still the water inside the tanks does not move as a solid body when the barge rolls. The roll inertia is lower than if the water were frozen; in our case, when related to the center-point of the tank, it is 65 % of the solid value.

Figures 2 and 3 show the experimental and numerical roll RAOs for the seastates Irr1 and Irr3. The computed ones are obtained with the 2D model, with viscous roll coefficients C_d of 0.12, 0.15 and 0.20. For the milder sea-state a good agreement is obtained with $C_d = 0.20$, while in the stronger one $C_d = 0.15$ gives the best fit. This suggests that the viscous damping moment in roll is not strictly quadratic with the roll velocity.

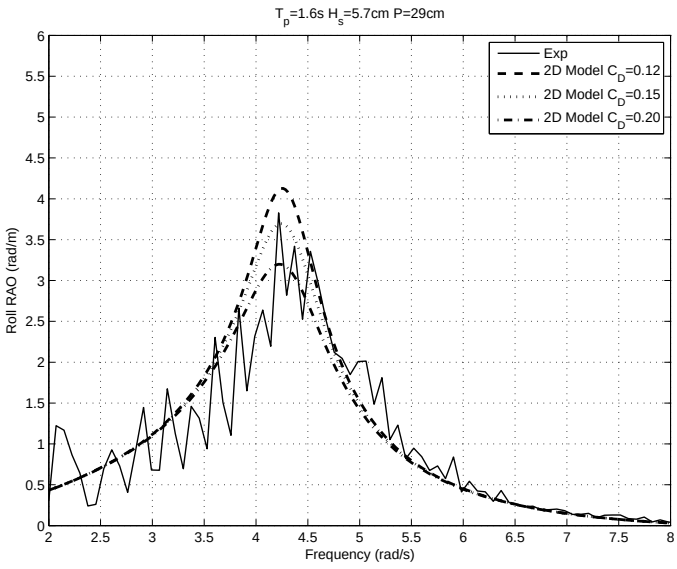

Figure 2. CLOSED TANKS. EXPERIMENTAL AND NUMERICAL ROLL RAOS. SEASTATE IRR1.

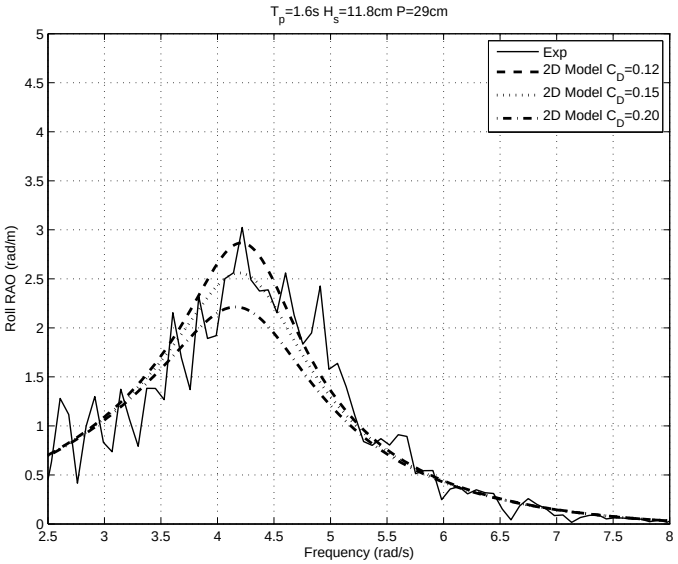

Figure 3. CLOSED TANKS. EXPERIMENTAL AND NUMERICAL ROLL RAOS. SEASTATE IRR3.

Flat roofs

In this section we consider the cases with the roofs flat (no chamfers). Three distances from the roofs to the mean free surface were considered in the tests, that is 6, 11 and 16 cm (configurations P35, P40 and P45). In the numerical model, which is linear (except for the roll viscous damping and the quadratic damping term in the tanks), there are no roofs. The question that we address here is to what extent the results given by our numerical model deviate from measurements as the roof clearance decreases. Rognebakke & Faltinsen [3] have proposed that roof impacts induce some damping of the sloshing motion; so it could be a matter of properly tuning the damping coefficients in the pendulum equations of the sloshing modes (35).

Roofs at 16 cm above water level Here we consider the roofs in their highest position (P45), 16 cm above the still water level.

Seastate Irr1 Figure 4 shows numerical and experimental RAOs of the barge roll motion, for the mildest seastate Irr1 ($H_S = 6$ cm, $T_P = 1.6$ s). In this seastate no roof impact was observed. Numerical RAOs have been obtained with the 2D model, with different amounts of viscous roll damping ($Cd = 0.15$ and $Cd = 0.20$), while the linear damping in the tanks is set at 0 or 2 % of critical damping. The best fit is obtained with $C_d = 0.20$ (as in the previous case) and no damping in the tank (in agreement with the results from the previous campaign — see [1]).

The video recording of the onboard camera (see figure 9) was processed in order to derive experimental RAOs of the am-

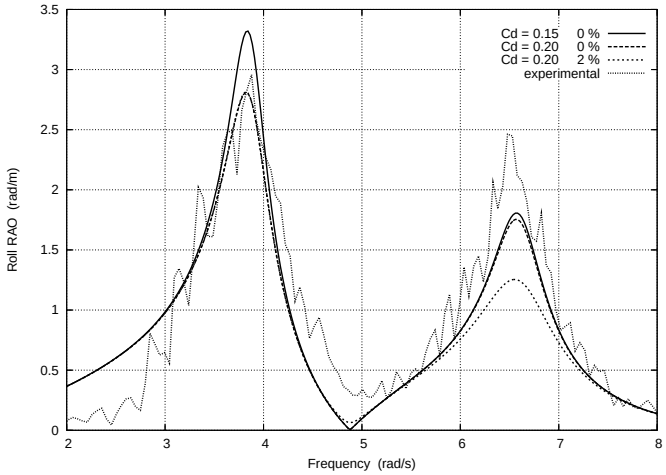

Figure 4. ROLL RAO. FLAT ROOF 16 CM ABOVE STILL WATER LEVEL. SEASTATE IRR1.

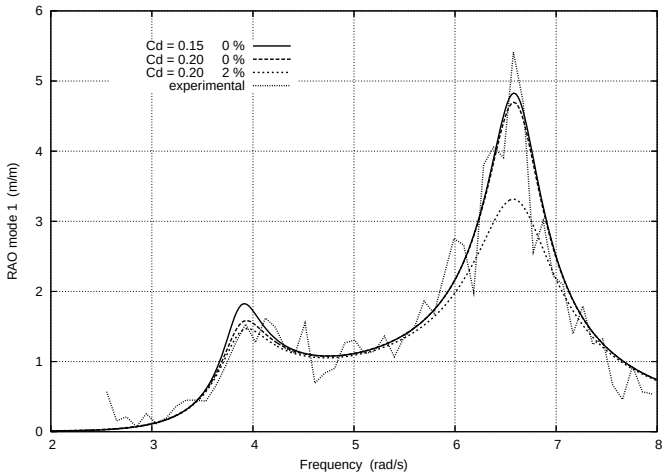

Figure 5. RAO OF THE FIRST SLOSHING MODE. FLAT ROOF 16 CM ABOVE STILL WATER LEVEL. SEASTATE IRR1.

plitudes of the sloshing modes. Figure 5 shows, for the same seastate Irr1, the experimental RAO of the first sloshing mode, compared with the computed ones. (This refers to the sloshing motion in the moving coordinate system, i.e. the modal amplitude A_1 is modified to account for the roll motion of the barge). As with the roll motion the best fit is obtained with no damping in the tanks.

Next figure 6 shows the RAO of the amplitude of the second odd mode ($n = 3$, the first even mode $n = 2$ being nil according to our linear model). Experimental and numerical values are only about 10 % of the first mode's. It can be observed that the experimental RAOs somewhat exceed the numerical ones, whatever the

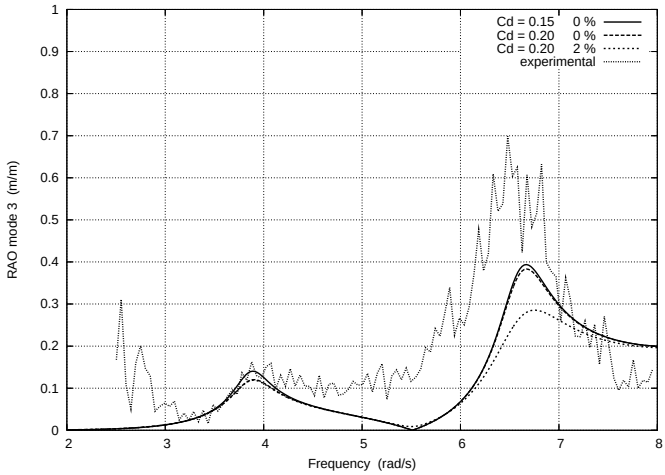

Figure 6. RAO OF THE SECOND ODD MODE. FLAT ROOF 16 CM ABOVE STILL WATER LEVEL. SEASTATE IRR1.

amount of damping. This discrepancy is presumably associated with free surface nonlinearities.

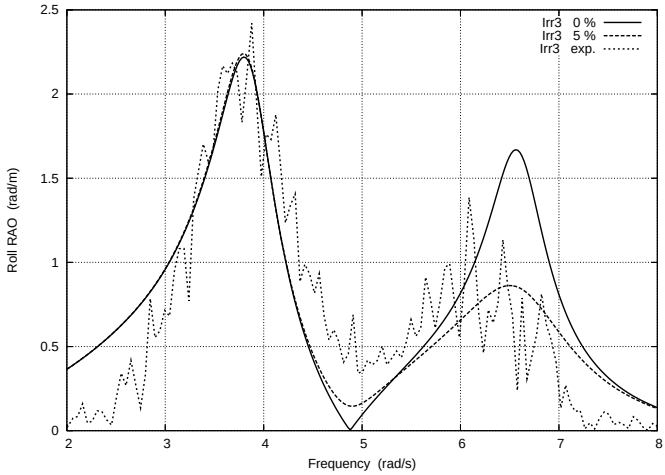

Figure 7. ROLL RAO. FLAT ROOF 16 CM ABOVE STILL WATER LEVEL. SEASTATE IRR3.

Seastate Irr3 Figure 7 shows the experimental roll RAO in seastate Irr3, and the computed ones with 0 and 5 % internal damping in the tanks. With 5 % damping the height of the second peak agrees well with the experimental one but the location is not correct: as compared to seastate Irr1 the experimental peak has shifted toward lower frequencies.

This can also be observed in figure 8 which shows the exper-

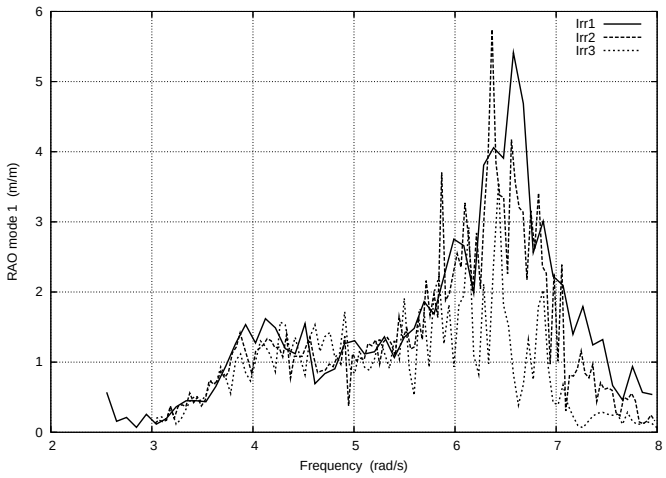

Figure 8. RAO OF THE FIRST SLOSHING MODE. FLAT ROOF 16 CM ABOVE STILL WATER LEVEL. SEASTATES IRR1, IRR2, IRR3.

imental RAOs of the first sloshing mode for the three seastates Irr1, Irr2 and Irr3. Noticeable are the shifts of the peaks toward lower frequencies, while the curves get flatter, as the severity of the seastates increases. The frequency shift may be attributed to nonlinear free surface effects: third-order theory predicts such frequency shifts (e.g. see [2]). In our numerical model this presumably could be accounted for by adding up nonlinear (cubic) restoring terms in the pendulum equations (35), rendering them Duffing-like.

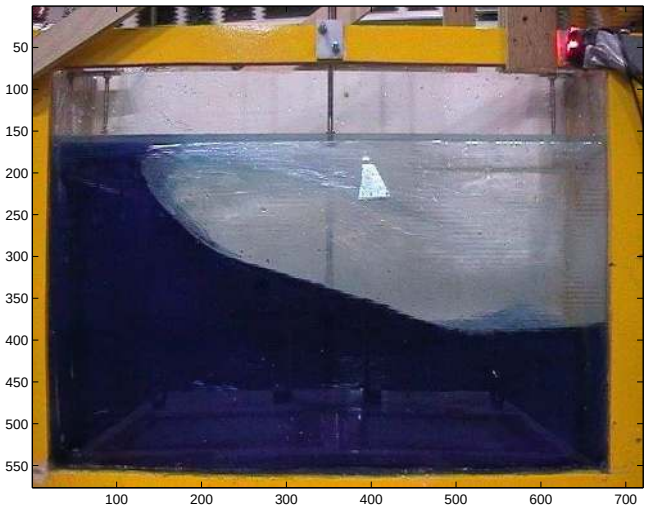

Figure 9. FLAT ROOF IN P40 CONFIGURATION. VIEW FROM THE ONBOARD VIDEO CAMERA (NUMBERS ARE PIXELS).

Other roof elevations Figure 9 shows a view of the tank, from the onboard video camera, with the flat roof 11 cm above the mean free surface.

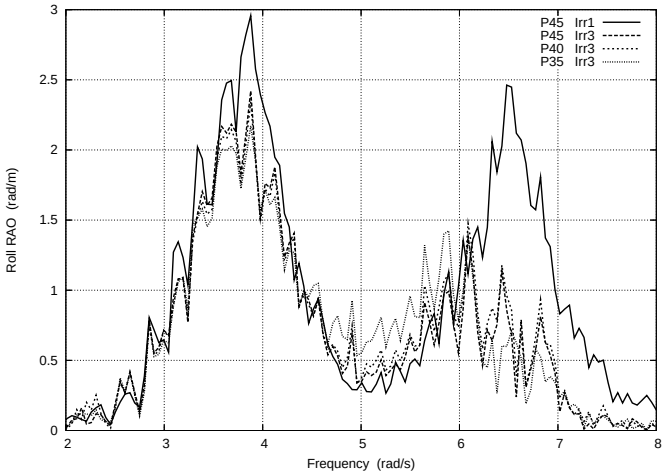

Figure 10. ROLL RAO FOR DIFFERENT ROOF ELEVATIONS.

In figure 10 we show the experimental RAOs of the roll motion in seastate Irr3 for the three positions of the roofs P45 (16 cm above free surface), P40 (11 cm above) and P35 (6 cm). The number of recorded roof impacts was, respectively, 27, 89 and 149 (over about 375 wave cycles). In the figure we also show, for reference, the experimental RAO in seastate Irr1 at the highest roof elevation (see figure 4). Surprisingly the first three curves are nearly coincident, despite the large differences in roof impacts.

This suggests that the decrease of the second peak of the roll RAO, when the seastate becomes stronger, is not only due to increasing energy dissipation but also to some other effects, probably associated with the nonlinearities in the free surface equations. This point deserves further investigation.

Chamfered roofs

Except for the configuration P50, the chamfers are penetrating the free surface. This means that the natural sloshing modes in the tanks cannot be determined analytically any more, so we use DIODORE^{TM}, both to compute the hydrodynamic characteristics of the barge (diffraction loads, added masses and dampings) and the sloshing modes and infinite frequency added masses of the tanks.

Figure 11 shows the mesh of the tank in the P35 configuration. Figure 12 shows a view of the chamfered tank from the onboard video camera.

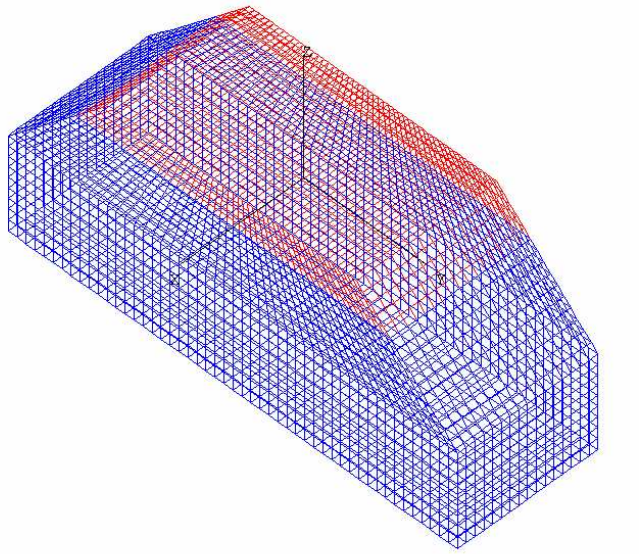

Figure 11. CHAMFERS AT 12 CM IMMERSION. MESH OF THE TANK.

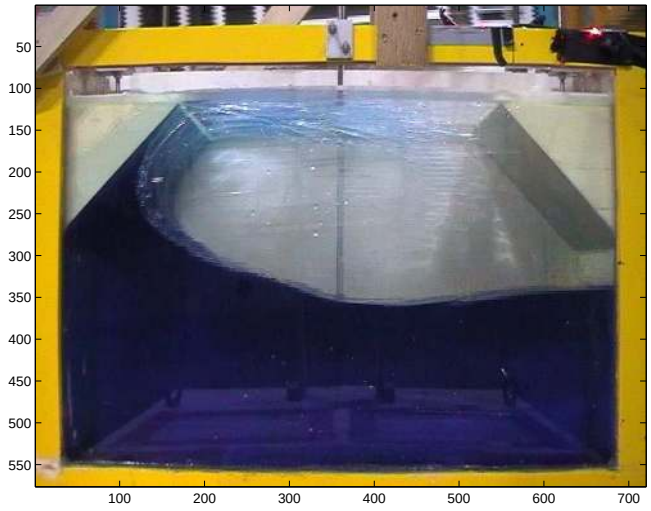

Figure 12. CHAMFERS IN P45 CONFIGURATION. VIEW FROM THE ONBOARD VIDEO CAMERA.

P45 configuration Figure 13 shows the experimental roll RAOs in the milder seastate Irr1, for the flat roof 16 cm above the mean free surface (P45) and for the P45 chamfered case. Numerical results are shown as obtained with the 2D model (which ignores the chamfers) and with DIODORE^{TM}. The presence of the chamfers, slightly reducing the length of the free surface, causes the second peak of the roll RAO, associated with the resonant sloshing motion in the tank, to shift toward the higher

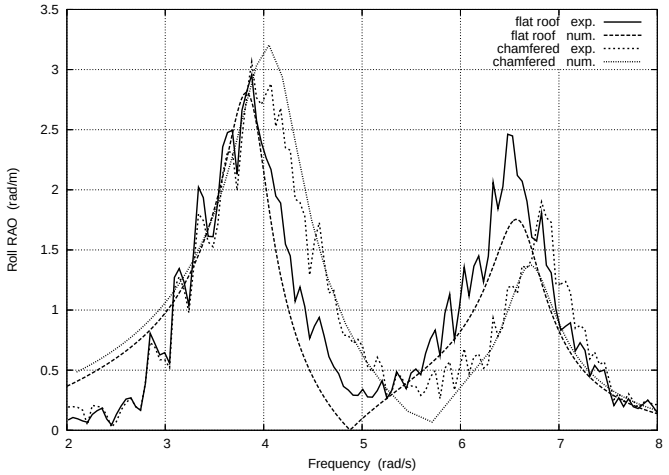

Figure 13. CONFIGURATION P45. SEASTATE IRR1. MEASURED AND CALCULATED ROLL RAOS.

frequencies, while it is somewhat reduced. The first peak is also slightly shifted. These features are well reproduced with DIODORE^{TM}.

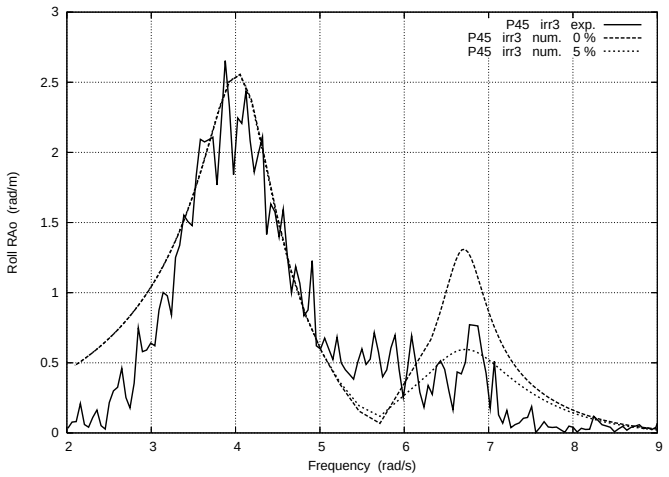

Figure 14. CONFIGURATION P45. SEASTATE IRR3. MEASURED AND CALCULATED ROLL RAOS.

Figure 14 refers to the seastate Irr3 and shows the experimental and numerical roll RAOs, obtained with 0 and 5 % internal damping. The second peak of the experimental RAO appears to be somewhat blurred and shifted toward lower frequencies. Again, like in the flat roof case, with 5 % internal damping, the peak level (if not the shape) is well rendered.

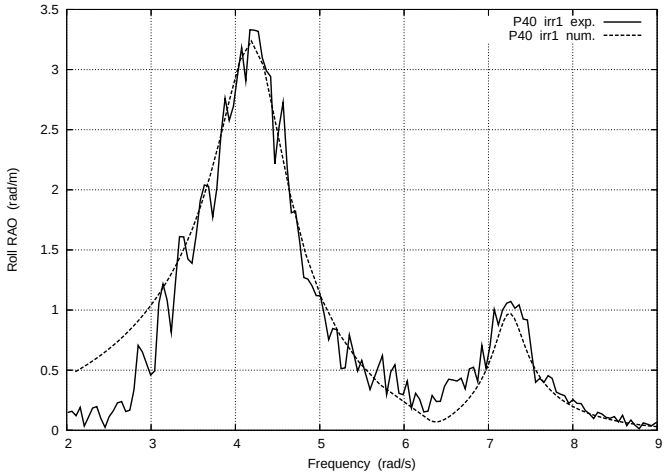

Figure 15. CHAMFERS 7 CM IN WATER. SEASTATE IRR1. MEASURED AND CALCULATED ROLL RAOS.

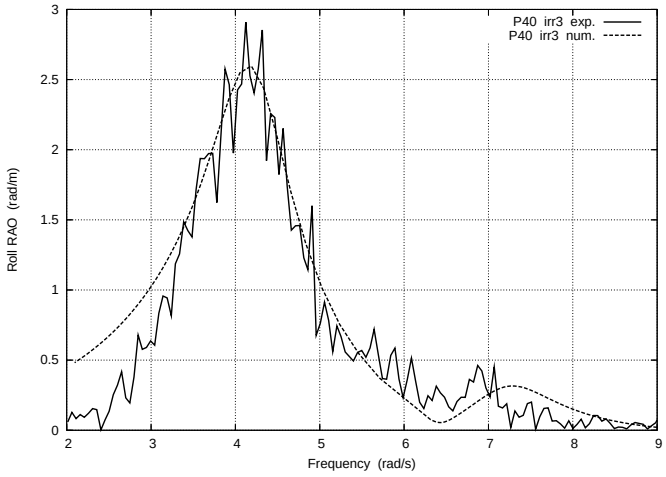

Figure 16. CHAMFERS 7 CM IN WATER. SEASTATE IRR3. MEASURED AND CALCULATED ROLL RAOS.

P40 configuration Figures 15 and 16 refer to the P40 case, meaning the bottom ends of the chamfers are 7 cm below the free surface, the length of which is reduced from 80 to 66 cm. Figure 15 shows the experimental and numerical roll RAOs, in the milder seastate Irr1. As a result of the reduced free surface length, the second peak has been shifted toward higher frequencies and reduced in size. Figure 16 refers to the seastate Irr3: the second peak, associated with the sloshing motion, has almost disappeared from the experimental RAO. In the calculations an internal damping of 5 % of critical has been added up (no additional damping was introduced in seastate Irr1).

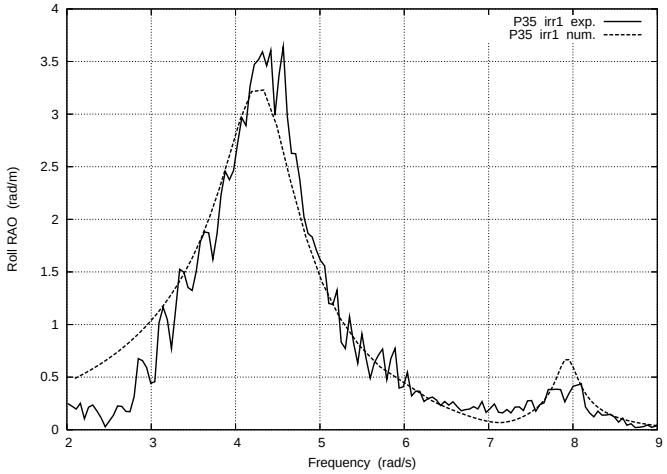

Figure 17. CHAMFERS AT 12 CM IMMERSION. SEASTATE IRR1. MEASURED AND CALCULATED ROLL RAOS.

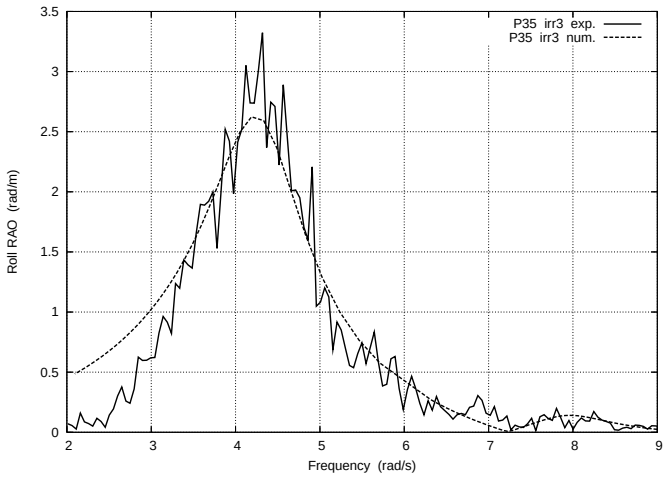

Figure 18. CHAMFERS AT 12 CM IMMERSION. SEASTATE IRR3. MEASURED AND CALCULATED ROLL RAOSs.

P35 configuration In the P35 configuration the chamfers are more deeply immersed and the free surface length is reduced to 56 cm. Figures 17 and 18 show the experimental and numerical roll RAOs in seastates Irr1 and Irr3, also with (respectively) 0 and 5 % internal damping. The natural frequency of the

first sloshing mode has shifted even higher and its effect on the barge roll motion has become hardly noticeable.

CONCLUSION

In mild seastates, good agreement has been reported between calculated and measured roll RAOs, whatever the shapes (flat or chamfered) and positions of the roofs. The energy dissipation that takes place in the tanks in insignificant.

As the seastate becomes more severe, nonlinear effects come into play: the second peak of the roll RAO decreases and flattens, while it shifts toward lower frequencies. Numerically the decrease and flattening can be rendered by introducing some energy dissipation in the tanks. Surprisingly hardly no difference can be observed in the experimental roll RAOs when the airgap between the flat roofs and the free surface varies, even though the number and intensity of roof impacts are very different. This suggests that the decrease of the second peak may not be so much due to internal dissipation than to free surface nonlinearities. This point deserves further investigations.

With chamfered corners, decreasing the airgap also means decreasing the free surface area and increasing the natural frequency of the sloshing motion. As a result the coupling effects between sloshing motion and roll response weaken.

These conclusions refer to the tested cases. They do not pretend to have any degree of generality when the geometries of the tanks and floating support, or filling ratios, vary.

REFERENCES

[1] B. Molin, F. Remy, S. Rigaud & C. de Jouette, 2002. LNG-FPSO's: frequency domain, coupled analysis of support and liquid cargo motions. In Proc. 10th IMAM Conference, Rethymnon.

[2] N. N. Moiseev, 1958. On the theory of nonlinear vibrations of a liquid of finite volume. *Applied Math. & Mech. (PMM)*, **22**, 5.

[3] O. F. Rognebakke & O. M. Faltinsen, 2000. Damping of sloshing due to tank roof impact. In Proc. 15th Intern. Workshop Water Waves & Floating Bodies, Caesarea (available at http://www.iwwwfb.org).

ACKNOWLEDGMENTS

The model tests were carried out within the GIS-HYDRO organization with financial support from Conseil Général du Var and from Saipem S.A. Their analysis was performed within the CEP&M project "Unités GNL Offshore".